


Slip avalanche in nanoscratching of metallic glasses

Cite as: J. Appl. Phys. **122**, 115108 (2017); <https://doi.org/10.1063/1.4989455>

Submitted: 09 June 2017 . Accepted: 05 September 2017 . Published Online: 20 September 2017

D. X. Han, G. Wang, J. L. Ren , S. X. Song, J. Li, J. Yi, Y. D. Jia, H. Xu, K. C. Chan, and P. K. Liaw



View Online



Export Citation



CrossMark

ARTICLES YOU MAY BE INTERESTED IN

[Evaluating the correlation between liquid fragility and glass-forming ability in the extremely strong Ce-based bulk metallic glasses](#)

Journal of Applied Physics **122**, 115107 (2017); <https://doi.org/10.1063/1.4996269>

[Flexible strain sensors with high performance based on metallic glass thin film](#)

Applied Physics Letters **111**, 121906 (2017); <https://doi.org/10.1063/1.4993560>

[Shocking of metallic glass to induce microstructure heterogeneity: A molecular dynamics study](#)

Journal of Applied Physics **122**, 095102 (2017); <https://doi.org/10.1063/1.5000366>

Lock-in Amplifiers
Find out more today



 Zurich Instruments

Slip avalanche in nanoscratching of metallic glasses

D. X. Han,¹ G. Wang,^{1,a)} J. L. Ren,² S. X. Song,³ J. Li,¹ J. Yi,¹ Y. D. Jia,¹ H. Xu,¹ K. C. Chan,⁴ and P. K. Liaw⁵

¹Laboratory for Microstructures, Institute of Materials, Shanghai University, Shanghai 200444, China

²School of Mathematics and Statistics, Zhengzhou University, Zhengzhou 450001, China

³State Key Laboratory of Metal Matrix Composites, School of Materials Science and Engineering, Shanghai Jiao Tong University, Shanghai 200240, China

⁴Department of Industrial and Systems Engineering, The Hong Kong Polytechnic University, Hong Kong, China

⁵Department of Materials Science and Engineering, The University of Tennessee, Knoxville, Tennessee 37996, USA

(Received 9 June 2017; accepted 5 September 2017; published online 20 September 2017)

Slip avalanches, similar to discrete earthquake events, of Zr-, Co-, and Ce-based metallic glasses during nanoscratching were investigated. Differing from the conventional continuum approach, mean-field theory, which is an inherently-discrete model, was applied to analytically compute intermittent slip avalanches. Mean-field theory was first connected with the potential energy barrier and concentration of free volume in order to study the stick-slip behavior. The results suggest that the motion behavior of free volume affects the critical slip avalanche size. *Published by AIP Publishing.* [<http://dx.doi.org/10.1063/1.4989455>]

I. INTRODUCTION

Originating from shear localization, instantaneously brittle failure restricts the application of metallic glasses (MGs),^{1–3} although they reveal outstanding engineering performances, such as high strength, high elastic limit, and strong corrosion resistance.^{4–9} On the other hand, the ductile deformation of MGs on the microscale,^{10,11} benefits from a decrease in the shear-band spacing with decreasing MGs size,¹² avoids macroscopic brittle properties and allows them to become a potentially structural material in the field of miniaturized devices. Thus, the mechanical performance of MGs on the microscale has recently drawn great attention. Compression and tension experiments on MG micro-samples were carried out to gain a fundamental understanding of the mechanical properties of MGs on the microscale.^{13–15} However, most reports on MGs' size-dependent mechanical properties are inconsistent for the artificial effects, e.g., the taper angle and top curvature of micropillars,^{16,17} and brittle-ductile transition induced by iron irradiation¹⁸ from focused ion beam (FIB) preparation. A nanoscratching test is a simple and effective method to investigate micromechanical properties of MGs^{19,20} and can avoid the above-mentioned artifacts.

Slip avalanches, arising from the stick-slip operation of shear band which is resulted from the free-volume accumulation,^{21–24} are investigated during nanoscratching. So far, slip avalanches, which impede the improvement of the plasticity and the toughness of MGs,²⁵ resulting in catastrophic fracture,⁴ have not received much attention in nanoscratching research, although they have been widely studied in the compressive deformation of MGs.^{26–28} Understanding and predicting the dependence of slip avalanches on the material and loading force are important for the elucidation of the stick-slip behavior of MGs on the microscale. The intermittent slip avalanche in nanoscratching is similar to the earthquake

event.²⁹ In the present study, mean-field theory,^{30,31} widely applied to earthquakes and based on discrete mechanics, is introduced to analyze the statistical properties of slip avalanches during nanoscratching. Based on the analysis of the dynamics, the activation energy of the free-volume arrangement and the critical and non-critical free-volume flow coefficient equations are developed.

II. EXPERIMENT

Three MGs, i.e., Ce₆₈Al₁₀Cu₂₀Co₂ (at. %, Ce-based), Zr_{41.25}Ti_{13.75}Ni₁₀Cu_{12.5}Be_{22.5} (at. %, Zr-based), and Co₅₆Ta₉B₃₅ (at. %, Co-based), were chosen for the model materials due to their significantly different mechanical properties. Ingots of the three MGs were prepared by arc melting a mixture of pure metal elements (purity $\geq 99.9\%$) in a Ti-gettered argon atmosphere. Each ingot was remelted at least four times, ensuring compositional homogeneity. Suction casting the ingots into a Cu-mould to form rod-like MGs. The rod-like MGs had a dimensional size of $\Phi 2 \text{ mm} \times 70 \text{ mm}$. Nanoscratch testing was conducted in a Triboindenter TI-900 machine (Hysitron, Inc.). The nanoscratching indenter was a conical diamond with a tip radius of $1 \mu\text{m}$ and half-angle of 30° . The load force and displacement resolution were 50 nN and $2 \times 10^{-2} \text{ nm}$, respectively. The scratch length was $20 \mu\text{m}$, and the moving speed of the nanoindenter was $1 \mu\text{m/s}$. The nanoscratch testing was conducted at different loading forces of 500 , 1000 , and $1500 \mu\text{N}$ in order to study the effect of loading force on the nanoscratching process in MGs. At each loading force, at least four scratches were repeatedly executed, and an air-scratch test was performed to obtain the background noise.

III. RESULTS AND DISCUSSION

A. Mean-field theory

The indenter penetrating depth, S_D , vs. scratch length, S_L , is shown in Fig. 1(a). The average indenter penetrating

^{a)}Author to whom correspondence should be addressed: g.wang@i.shu.edu.cn

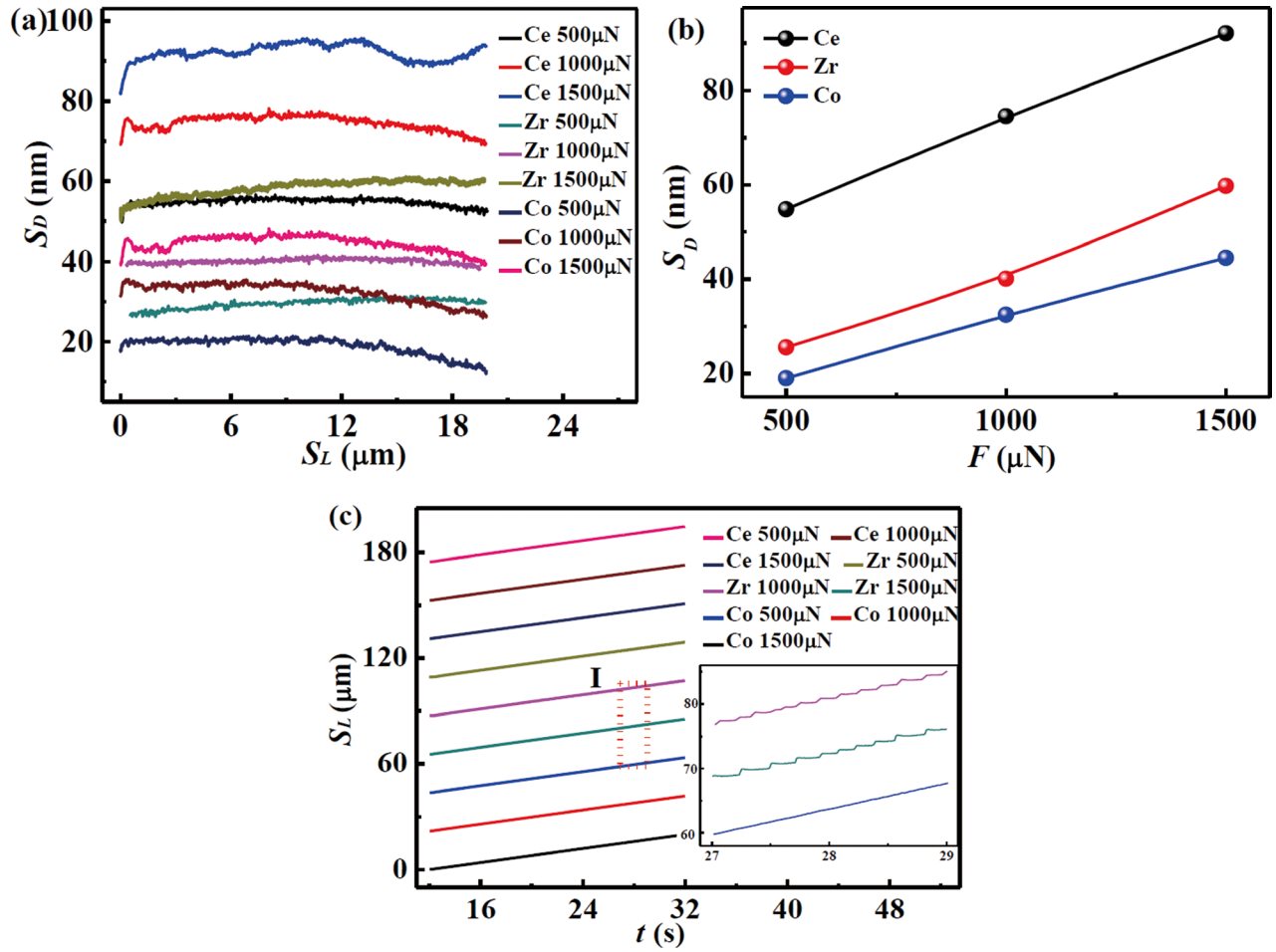


FIG. 1. Profile of the nanoscratching process. (a) The indenter penetrating depth during nanoscratching for Ce-, Zr-, and Co-based MGs. (b) The indenter penetrating depths vs. loading forces for Ce-, Zr-, and Co-based MGs. (c) The scratch length vs. time for Ce-, Zr-, and Co-based MGs. Inset is the enlarged view of region I, which shows the serration event.

depth increases with increasing loading force, as shown in Fig. 1(b). The scratching length, S_L , as a function of time, t , is plotted in Fig. 1(c). The enlarged S_L - t curve shows that some serrations, which are the so-called slip avalanches, can be observed in the insert of Fig. 1(c). With increase in the loading force, the slip avalanche becomes more obvious.

To effectively study the underlying process of the slip avalanche, a linear function is used to fit the nanoscratching process in the S_L - t curve to obtain a baseline, as shown in Fig. 2(a). The S_L fluctuations can be observed clearly after enlarging the S_L - t curve that is enclosed in the rectangle in Fig. 2(a). After subtracting the baseline, the avalanche event is characterized by the repeated displacement increases and decreases, as shown in Fig. 2(b). The difference between the peak and valley displacement, ΔH , reflects the avalanche size. Since the background noise from the machine vibration induces perturbations in the displacement, an air nanoscratching test was carried out, and the background noise was calculated to be $4.90 \times 10^{-3} \mu\text{m}$ (see the [supplementary material](#)). Thus, ΔH values less than $4.90 \times 10^{-3} \mu\text{m}$ are excluded. Due to the system-inherent parameters of Triboindenter TI-900 machine, the loading force has an increasing trend in the nanoscratching process, causing the avalanche size to increase with time during the experiments. It induces a systematic drift of the

serration amplitude. Normalization of the ΔH value was carried out to exclude the system deviation.³² A linear regression equation was fitted to the ΔH value vs. time plot, and $f(t_0)$ is fitted at the starting time, t_0 , as shown in Fig. 2(c). The normalized ΔH value, $S = \frac{\Delta H}{f(t)/f(t_0)}$, as a function of time, is shown in Fig. 2(d). The statistics of the S values were used to characterize the essential dynamics of the stick-slip in the nanoscratching. The probability distributions of the normalized avalanche size, S , i.e., the percentages of the S values being larger than a given value, $P(>S)$, for three MGs at three loading forces (500, 1000, and 1500 μN), are shown in Fig. 3. The slip avalanche distributions can be modeled by a squared exponential decay function as follow:^{33,34}

$$P(>S) = AS^{-(k-1)} \exp[-(S/S_C)^2], \quad (1)$$

where A is a normalization constant, κ is a scaling exponent ($\kappa = 1.5$ in mean-field theory), and S_C is the cut-off value of the slip avalanche, acting as the critical slip avalanche size. The critical avalanche sizes of the three MGs are listed in Table I.

Metallic glasses have intrinsic structural heterogeneity for specific local-atomic arrangements giving rise to clusters with a lower shear modulus.³⁵⁻³⁸ The heterogeneous structures, i.e.,

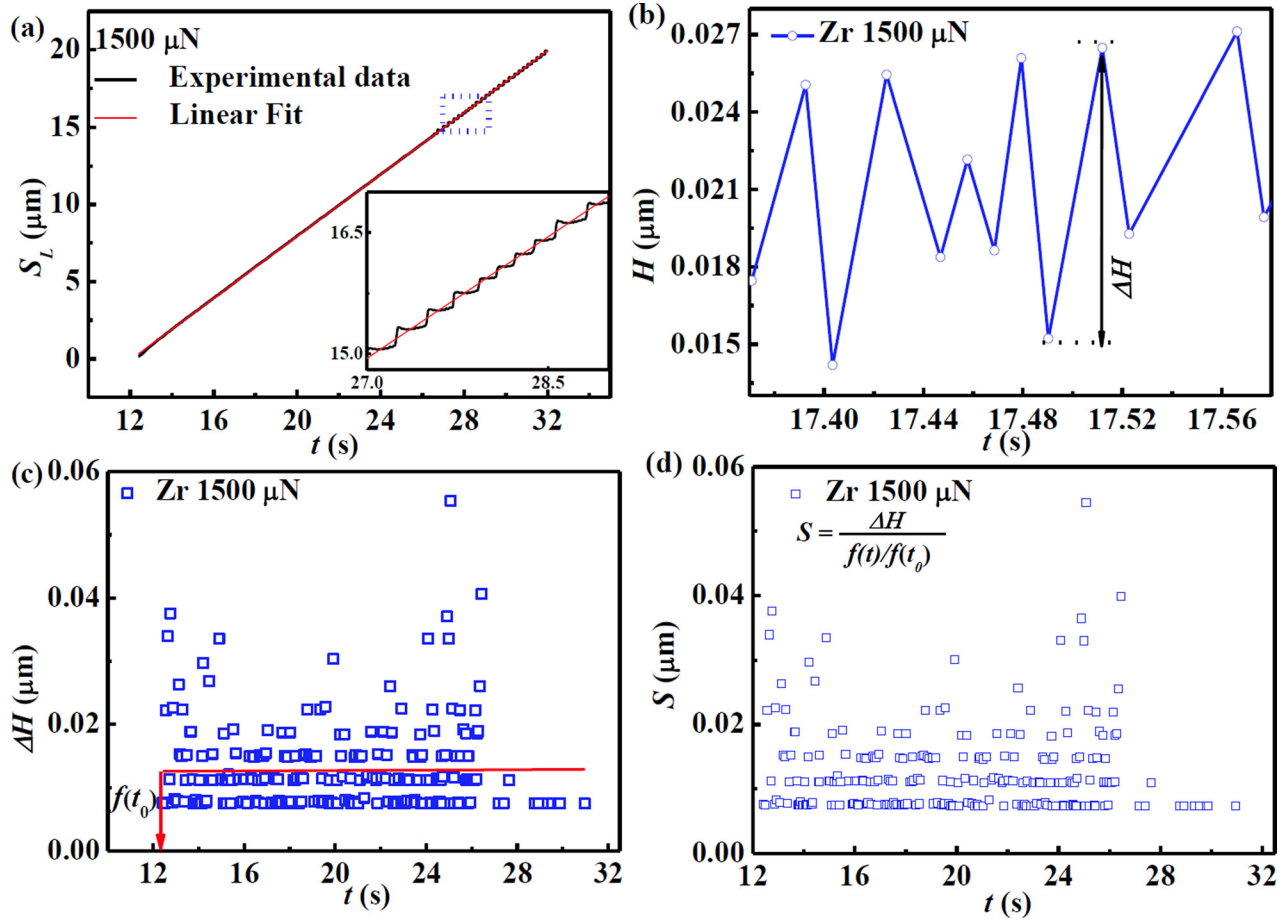


FIG. 2. Slip avalanche during the nanoscratching process. (a) An example of the slip avalanche event taken from the scratch length vs. time curve of Zr-based MG at a loading force of $1500 \mu\text{N}$. Linear function fitting curve of scratch length vs. time. The inset shows the enlarged scratch length vs. time curve. (b) Slip avalanche event after subtract the baseline. (c) Scratch length burst size vs. time. The red line is the average scratch length burst size obtained by linearly regression fitting. (d) The normalized scratch length burst size vs. time.

free volumes with high atomic mobility in MGs, are easier to be shear deformed than the glassy phases surrounding these heterogeneous structures, which can be regarded as the weak spots during slip avalanching. When the forces are applied to the system, the elastic energy from the external force is stored until the local force surpasses a threshold value. Then, the free volumes are formed and the stored energy released, balancing the energy increment from the external force. During the slip process, the released energy is redistributed to the neighboring free volume. Thus, the operation of one free volume may trigger other free volumes to concordantly operate, which resembles a domino effect. The phenomenon contributes to the forming of slip avalanches of different sizes. Two types of avalanche size distribution are recognized in Fig. 3. When $S \ll S_C$, the statistical distribution of the serration size follows a power-law relationship. Although the localized free volumes usually yield a Gaussian like probability distribution, the activated free volumes are highly connected with each other through elastic interaction, leading to slip avalanches of different sizes, scaled as a power-law distribution.^{39,40} When $S \gg S_C$, the P value decays exponentially because the discreteness effects of the weak spot come into play.⁴¹ The exponential distribution suggests a chaotic behavior, which indicates that the serrations are sensitive to the external perturbation, e.g., the external force, causing catastrophic failure.⁴² The S_C

value varies with different MGs and increases with increasing loading force. The scaling exponents of the three MGs at different loading forces are almost same (1.20 ± 0.19) and deviate from the typical value (1.5) used in mean-field theory. The deviation is correlated with the dimensional difference, as well as statistical fluctuations. Usually, the scaling exponent is associated with the Gutenberg-Richter power-law exponent, b , $b = 3 \frac{(\kappa-1)}{2}$,^{43,44} which varies with the spatial dimension. For the two dimensions, the b value is 0.4 and for three dimensions, $b = 0.6$.⁴⁵ Correspondingly, the κ values are 1.26 in two-dimensional space and 1.40 in three-dimensional space, respectively. The nanoscratching in the current experiments can be taken as two-dimensional. Thus, the mean scaling exponent in our work deviates from 1.5 and is nearer to 1.2. Furthermore, the κ value is not affected by the variation of the S_C value, irrespective of the length scale and material structure.

B. Potential-energy barrier analysis

When an MG is scratched, the released stress is redistributed to the free volume in the system. The redistribution stress causes free-volume rearrangement, which leads to a slip avalanche, affecting the value of S_C . The potential-energy barrier for the unstressed free-volume arrangements can be described as following:^{46,47}

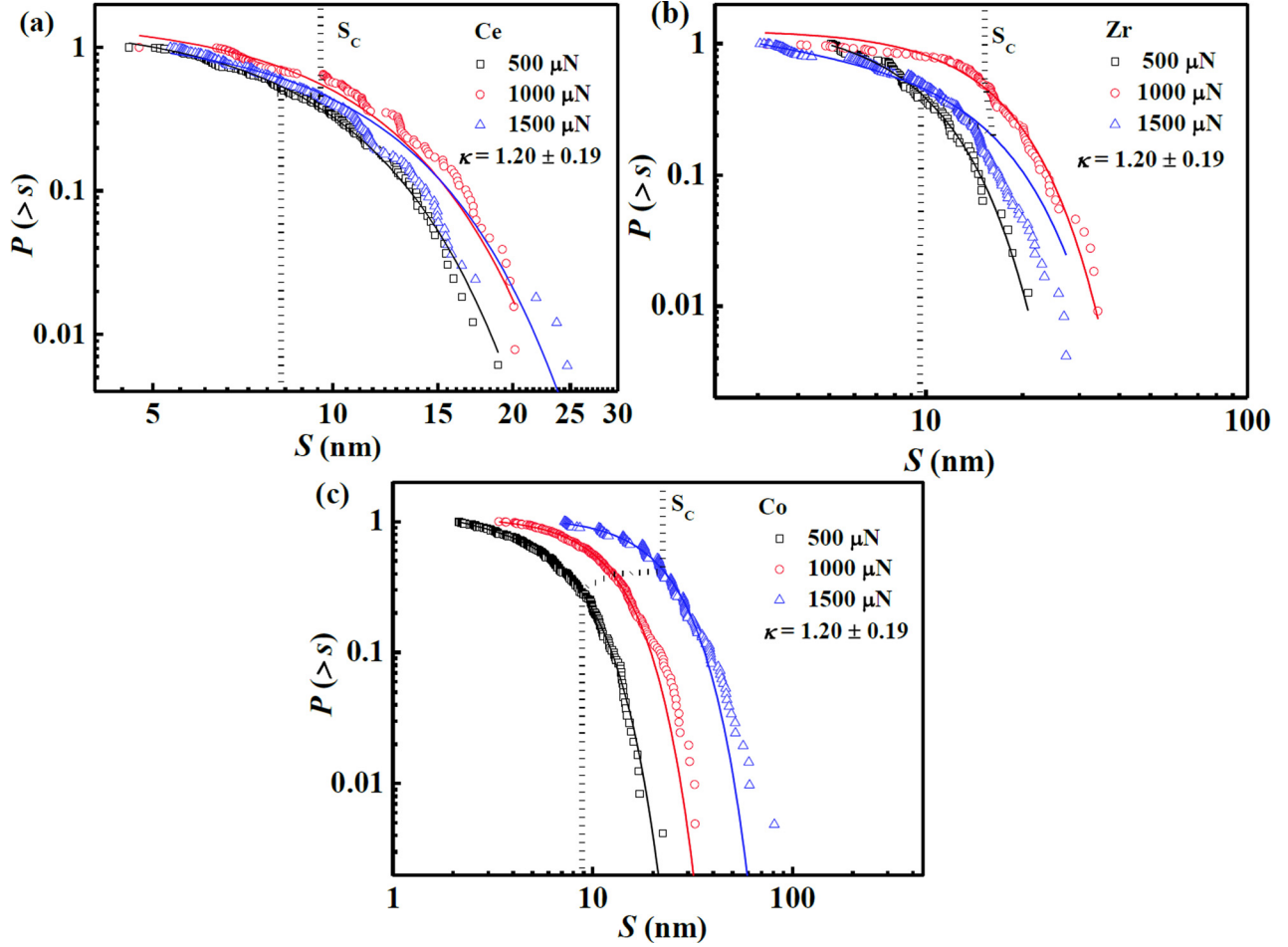


FIG. 3. Complementary cumulative probability distribution of the scratch length burst size. Solid lines are the fitting curves by Eq. (1). (a) Ce-based MG, (b) Zr-based MG, and (c) Co-based MG.

$$\Delta G^m = \frac{8}{\pi^2} G \gamma_C^2 \xi \Omega_s, \quad (2)$$

where ΔG^m is the activation energy of free-volume motion, G is the shear modulus, $\gamma_C \approx 0.027$ is the average elastic limit, $\xi \approx 3$ is a correction factor arising from the matrix confinement of a “stressed” atomic cluster, M is the molar mass, ρ is the density, and N_0 is Avogadro’s number. $\Omega_s \approx 2v^*$, where $v^* \approx M/(\rho N_0)$, is the average atomic volume. The parameters for the three metallic glasses are listed in Table II. Equation (2) originates from the potential energy barrier for the cooperative motion of the atomic clusters, termed as shear transformation zones (STZs). Both STZ theory and free-volume theory share the same idea that the locally cooperative motion of the atoms originates from the heterogeneous structures of MGs, and the flow event is initiated from the rearrangement of the atoms in local regions.^{15,51,52} Therefore,

the activation energy of an STZ can be applied to evaluate the activation energy of the free volume. Interested readers may refer to reference 44 for more details about the potential-energy barrier for free-volume motion.

The S_c value increases with increasing activation energy of free-volume motion, as shown in Fig. 4. The increment of the activation energy for the free-volume rearrangement indicates that the deformation requires more elastic energy.^{36,53} It suggests that a large elastic deformation zone, which contributes to a relatively long-range slip length, is required to compensate for the large activation energy. Therefore, the large activation energy corresponds to a large slip distance that leads to the large S_c value. For a certain activation energy, the S_c value increases with increasing loading force, which can induce the expansion of the free volume.^{35,54–56} With increasing stress, the expansion of free volume can allow the free volumes to encounter each other easily. The stronger connection

TABLE I. Critical slip avalanche sizes for three metallic glasses.

Metallic glasses	S_c (nm)		
	500	1000	1500
Ce-based	8.34	9.66	10.35
Zr-based	9.63	14.81	15.61
Co-based	10.14	16.54	23.60

TABLE II. Data of density, ρ , molar mass, M , average atomic volume, v^* , Poisson’s ratio, ν , and shear modulus, G , of three metallic glasses (Refs. 48–50).

Metallic glass	ρ (10^6 g/m ³)	M (g/mol)	v^* (10^{-29} m ³)	G (GPa)
Ce-based	6.752	111.900	2.752	11.8
Zr-based	5.900	60.041	1.690	34.1
Co-based	9.265	53.180	0.953	91.5

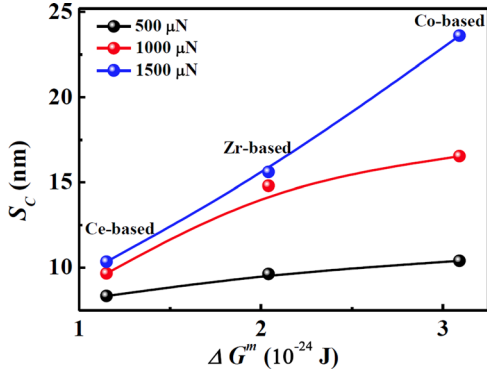


FIG. 4. The critical slip avalanche size vs. activation energy for the free-volume arrangement.

between the free volumes contributes to the sliding, with a larger distance, forming a larger S_c . To understand the influence of the loading force on the free-volume motion quantitatively, a free-volume flow coefficient is introduced.

C. Free-volume flow analysis

Nanoscratching behavior can be taken as a transient cutting process.⁵⁷ Derived from the similar shear-branching process,⁵⁸ the stick-slip behavior in nanoscratching corresponds to the shear localization in cutting. A vital factor for the system stability in MG cutting, η_c , is introduced to characterize the barrier for the flow of the free volume during the slip process^{59,60}

$$\eta_c = \left(\Lambda - \frac{4}{\alpha\phi \left(\xi_0 + \sqrt{\xi_0^2 + \frac{4\dot{\gamma}_{avg}}{\alpha\phi\eta_c}} \right)^3} \right) \dot{\gamma}_{avg}, \quad (3)$$

where η_c is the critical free-volume flow coefficient; Λ is a dimensionless shear modulus; α is the half-angle of the indenter ($\pi/6$). $\phi = \frac{2}{3} \times \frac{1+\nu}{1-\nu} \times \frac{\nu_h}{\nu^*} \times \frac{G}{\tau_0}$, where ν is the Poisson's ratio, ν_h is the critical volume of the effective hard-sphere atom, ν^* is the average atomic volume, and ξ_0 is the free-volume concentration outside of the primary shear zone. $\tau_0 = k_B T_0 / \nu^*$, where k_B is the Boltzmann constant and T_0 is the temperature outside the primary shear zone. $\dot{\gamma}_{avg}$ is the average strain rate applied to the primary shear zone. $\dot{\gamma}_{avg} = \nu_s / h$, where ν_s is the shear velocity and h is the thickness of the primary shear zone. The parameter ν_s is associated with the slip rate of the nanoindenter, ν , i.e., $\nu_s = \nu \times \cos\alpha = \nu \times \cos(\pi/6)$ (see the [supplementary material](#)). Since the ν value in the present study is $1 \mu\text{m/s}$, the ν_s value is calculated to be $0.866 \mu\text{m/s}$. For a certain MG, Λ , ϕ , α and ξ_0 are constants. Combining the parameters and Eq. (3) yields the following characteristic equation:

$$g_{(\eta_c, h)}^4 + a \times g_{(\eta_c, h)}^3 + b \times g_{(\eta_c, h)}^2 + c \times g_{(\eta_c, h)} + d = 0, \quad (4)$$

where $g_{(\eta_c, h)} = \xi_0 + \sqrt{\xi_0^2 + \frac{2\sqrt{3}}{\alpha\phi\eta_c}}$ is obtained from the substitution approach in calculating Eq. (4).

In the quartic Eq. (4), the $g_{(\eta_c, h)}$ is calculated to be $g_{(\eta_c, h)1} = \xi_0 + m$, $g_{(\eta_c, h)2} = \xi_0 - m$, $g_{(\eta_c, h)3} = -n + ei$, $g_{(\eta_c, h)4} = -n - ei$. The m , n , and e values are constants that are equal to or higher than 0. Hence, $g_{(\eta_c, h)1} = \xi_0 + m$ is a suitable value for Eq. (3), and the relationship between η_c and h can be expressed as

$$\eta_c \times h = A, \quad (5)$$

where A is a constant that depends on the parameter of MG

$$h = \frac{S_D}{2}, \quad (6)$$

where S_D is the indenter-penetrating depth. Combining Eqs. (5) (Ref. 59) and (6) produces a relationship between η_c and S_D

$$\eta_c \times S_D = B, \quad (7)$$

where B is a constant that depends on the parameter of MG.

The free-volume flow coefficient, η , which characterizes the dynamic evolution of free volume of MG,⁶¹ is introduced

$$\eta = \left(\frac{v_f + \frac{4D}{h}}{h} \right), \quad (8)$$

where v_f is a chip velocity, $v_f = \nu \times \sin\alpha = (1 \mu\text{m/s}) \times \sin(\pi/6) = 0.5 \mu\text{m/s}$ (see the [supplementary material](#)). D is the diffusion coefficient of the free volume, which is affected by temperature but is independent of stress. Combining Eqs. (6) and (8), a relationship between η_c and S_D can be expressed as

$$\eta = \left(\frac{1 + \frac{16D}{S_D}}{S_D} \right), \quad (9)$$

The difference between the free-volume flow coefficient, η , and the critical free-volume flow coefficient, η_c , is calculated to examine the effect of the free volume on the critical slip avalanche, i.e.,

$$\Delta\eta = \eta - \eta_c = \frac{C \times S_D + 16D}{S_D^2}. \quad (10)$$

where $C = (1 - B)$ is a constant and is dependent on the parameter of MG.

The $\Delta\eta$ value is a parameter reflecting the stability of the MG system in nanoscratching and depends on the material properties and the scratch depths. As shown in Fig. 5, the critical slip avalanche size decreases with increasing $\Delta\eta$ for the three MGs. The $\Delta\eta$ value is related to the effective change rate of the free volume.⁵⁹ In MGs, the rate of free-volume change can be divided into two processes, i.e., free-volume creation and annihilation.^{35,62} Free-volume creation, which is a stress-driven process, is induced by the stress squeezing an atom into a hole smaller than itself. The free-volume creation is slow at low stress and fast at high stress. Free-volume annihilation mostly depends on the temperature and is induced by a series of atomic diffusion jumps. The

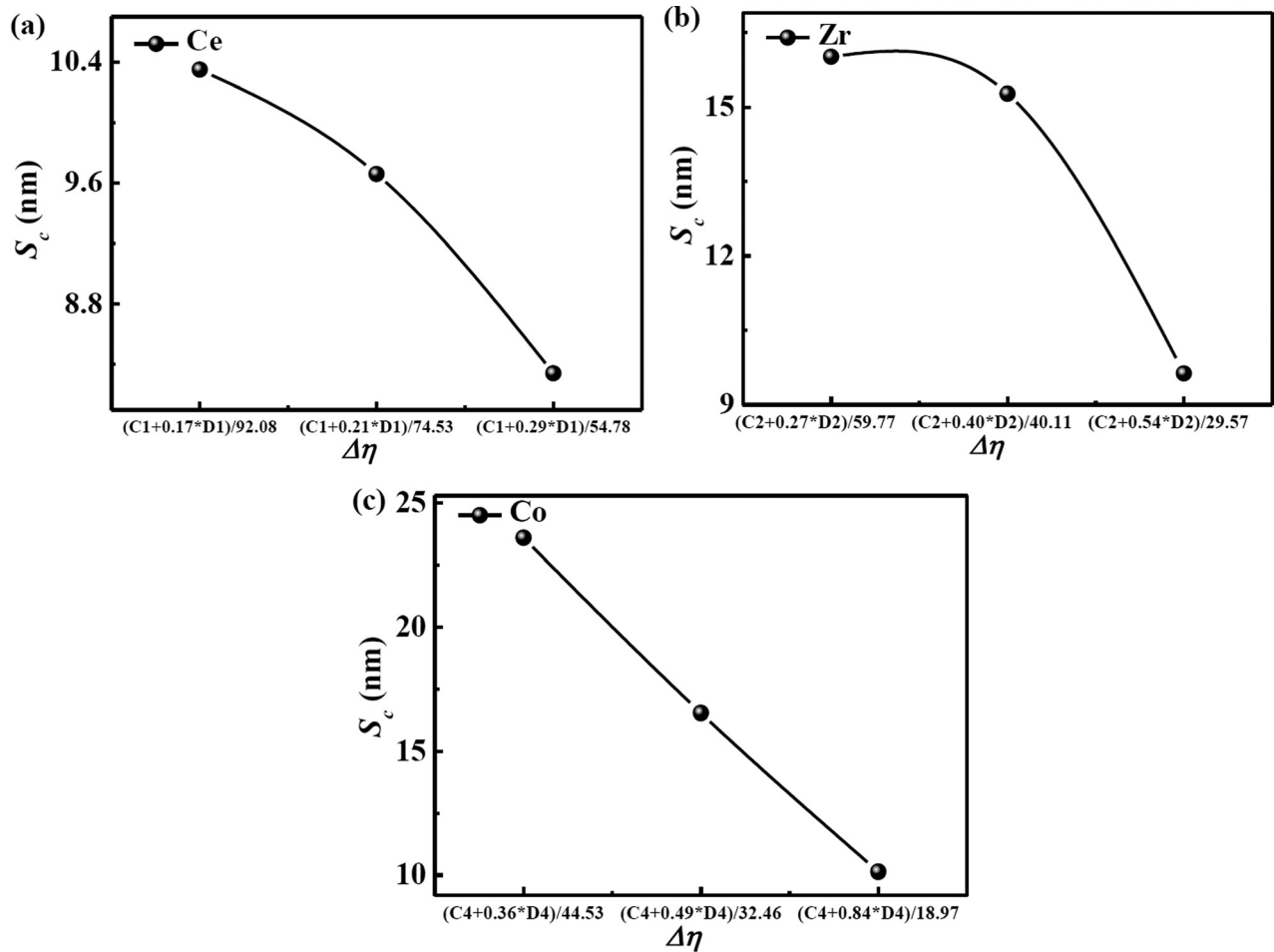


FIG. 5. The critical slip avalanche size vs. parameters for the stability of MG systems (a) Ce-based MG, (b) Zr-based MG, and (c) Co-based MG.

free-volume annihilation is slow at low temperature and fast at high temperature. The effective change rate of the free volume is the combined rate of the creation and annihilation of the free volume, i.e., the concentration of the free volume. In this case, the $\Delta\eta$ value is associated with the free-volume concentration in the present study. For a certain MG during the nanoscratching process, the increased loading force causes the contact area between the nanoindenter and the MG to augment, resulting in an increase in the friction force that improves the lateral force. The increased lateral force leads to an increase in the free-volume creation per unit time. The rate of free-volume annihilation remains the same for a certain MG at room temperature. Thus, the large loading force contributes to a large free-volume concentration, which corresponds to a small $\Delta\eta$ value. When a perturbation is applied to the MG, the free volume tends to dissipate the perturbation by spreading it to the adjacent free volumes in a chain reaction, until the free volumes become independent of each other.^{34,39} A larger free-volume concentration indicates that the communication among free volumes is stronger, being less hindered by the stable zone of low atomic liquidity. Thus, a large free-volume concentration can eliminate the perturbation in a relative long length scale, contributing to a large critical slip avalanche. A smaller $\Delta\eta$ value with a large free-volume concentration means that the system has a high disturbance resistance.

IV. CONCLUSION

In summary, mean-field theory was applied in this study, and it was found that the behaviors of the free volume, such as the potential-energy barrier for free-volume arrangements and free-volume concentration, affect the critical slip avalanche size. An MG with a large potential-energy barrier indicates a large critical slip avalanche size. Analysis of the difference between the free-volume flow coefficient and the critical free-volume flow coefficient, $\Delta\eta$, was developed to reflect the effective free-volume concentration. A small $\Delta\eta$ value suggests that the system has a good capability in its resistance to a disturbance, and contributes to a large critical avalanche size in regard to slip behavior.

SUPPLEMENTARY MATERIAL

See [supplementary material](#) for the background noise measurement, and details of the nanoindenter.

ACKNOWLEDGMENTS

The work described in this paper was supported by grants from the National Key Basic Research Program from MOST (No. 2015CB856800), the NSFC (Grant Nos. 51671120, 51501106, and 11771407), the Plan for Scientific Innovation Talent of Henan Province (No. 164200510011), Innovative Research Team of Science and Technology in

Henan Province (No. 17IRTSTHN007), the National Key Research and Development Program of China (No. SQ2017YFGX090043), the China Postdoctoral Science Foundation (No. 2016M601563), the Natural Science Foundation of Shanghai (No. 17ZR1440800), and the 111 project (No. D16002).

- ¹X. K. Xi, D. Q. Zhao, M. X. Pan, W. H. Wang, Y. Wu, and J. J. Lewandowski, *Phys. Rev. Lett.* **94**, 125510 (2005).
- ²J. J. Lewandowski, W. H. Wang, and A. L. Greer, *Philos. Mag. Lett.* **85**, 77 (2005).
- ³Z. F. Zhang, G. He, J. Eckert, and L. Schultz, *Phys. Rev. Lett.* **91**, 045505 (2005).
- ⁴M. F. Ashby and A. L. Greer, *Scr. Mater.* **54**, 321 (2006).
- ⁵J. Eckert, J. Das, S. Pauly, and C. Duhamel, *J. Mater. Res.* **22**, 285 (2007).
- ⁶U. Ramamurty, Y. Jana, Y. Kawamura, and K. Chattopadhyay, *Acta Mater.* **53**, 705 (2005).
- ⁷W. H. Wang, C. Dong, and C. H. Shek, *Mater. Sci. Eng. R* **44**, 45 (2004).
- ⁸W. H. Peter, R. A. Buchanan, C. T. Liu, P. K. Liaw, M. L. Morrison, J. A. Horton, C. A. Carmichael, and J. L. Wright, *Intermetallics* **10**, 1157 (2002).
- ⁹L. Huang, Z. Cao, H. M. Meyer, P. K. Liaw, E. Garlea, J. R. Dunlap, T. Zhang, and W. He, *Acta Biomater.* **7**, 395 (2011).
- ¹⁰D. Jang and J. R. Greer, *Nat. Mater.* **9**, 215 (2010).
- ¹¹D. Jang, C. T. Gross, and J. R. Greer, *Int. J. Plasticity* **27**, 858 (2011).
- ¹²D. Tönnies, R. Maaß, and C. A. Volkert, *Adv. Mater.* **26**, 5715 (2014).
- ¹³H. Guo, P. F. Yan, Y. B. Wang, J. Tan, Z. F. Zhang, M. L. Sui, and E. Ma, *Nat. Mater.* **6**, 735 (2007).
- ¹⁴J. Y. Kim, X. Gu, M. Wraith, J. T. Uhl, K. A. Dahmen, and J. R. Greer, *Adv. Funct. Mater.* **22**, 1972 (2012).
- ¹⁵R. Maaß and J. F. Löffler, *Adv. Funct. Mater.* **25**, 2353 (2015).
- ¹⁶O. V. Kuzmin, Y. T. Pei, C. Q. Chen, and J. T. M. De Hosson, *Acta Mater.* **60**, 889 (2012).
- ¹⁷M. C. Liu, J. C. Huang, K. W. Chen, J. F. Lin, W. D. Li, Y. F. Gao, and T. G. Nieh, *Scr. Mater.* **66**, 817 (2012).
- ¹⁸R. Cerling, F. P. Schimansky, and R. Wanger, *Acta Metall.* **35**, 1001 (1987).
- ¹⁹Q. Yuan, N. Ramisetti, and R. D. K. Misra, *Acta Mater.* **56**, 2089 (2008).
- ²⁰H. Ni, X. Li, H. Guo, and T. P. Nguyen, *Nanotechnology* **16**, 1746 (2005).
- ²¹R. Maaß, D. Klaumünzer, and J. F. Löffler, *Acta Mater.* **59**, 3205 (2011).
- ²²F. H. D. Forre, A. Dubach, J. Schällibaum, and J. F. Löffler, *Acta Mater.* **56**, 4635 (2008).
- ²³Y. J. Wang, M. Q. Jiang, Z. L. Tian, and L. H. Dai, *Scr. Mater.* **112**, 37 (2016).
- ²⁴Y. Shao, G. N. Yang, K. F. Yao, and X. Liu, *Appl. Phys. Lett.* **105**, 181909 (2014).
- ²⁵G. Wang, K. C. Chan, L. Xia, P. Yu, J. Shen, and W. H. Wang, *Acta Mater.* **57**, 6146 (2009).
- ²⁶D. M. Walker, A. Tordesillas, M. Small, and R. P. Behringer, *Chaos* **24**, 013132 (2014).
- ²⁷B. A. Sun and W. H. Wang, *Prog. Mater. Sci.* **74**, 211 (2015).
- ²⁸J. O. Krisponeit, S. Pitikaris, K. E. Avila, S. Küchemann, A. Krüger, and K. Samwer, *Nat. Commun.* **5**, 3616 (2014).
- ²⁹F. P. Landes, *Viscoelastic Interfaces Driven in Disordered Media* (Springer International Publishing, 2016).
- ³⁰K. A. Dahmen, D. Ertaş, and Y. Ben-Zion, *Phys. Rev. E* **58**, 1494 (1998).
- ³¹J. M. Schwarz and D. S. Fisher, *Phys. Rev. Lett.* **87**, 096107 (2001).
- ³²B. A. Sun, S. Pauly, J. Tan, M. Stoica, W. H. Wang, U. Kühn, and J. Eckert, *Acta Mater.* **60**, 4160 (2012).
- ³³N. Friedman, A. T. Jennings, G. Tsekenis, J. Y. Kim, M. Tao, J. T. Uhl, J. R. Greer, and K. A. Dahmen, *Phys. Rev. Lett.* **109**, 095507 (2012).
- ³⁴J. T. Uhl, S. Pathak, D. Schorlemmer, X. Liu, R. Swindeman, B. A. W. Brinkman, M. L. Blanc, G. Tsekenis, N. Friedman, R. Behringer, D. Denisov, P. Schall, X. Gu, W. J. Wright, T. Hufnagel, A. Jennings, J. R. Greer, P. K. Liaw, T. Becker, G. Dresen, and K. A. Dahmen, *Sci. Rep.* **5**, 16493 (2015).
- ³⁵F. Spaepen, *Acta Metal.* **25**, 407 (1977).
- ³⁶A. S. Argon, *Acta Metal.* **27**, 47 (1979).
- ³⁷J. Ding, Y. Q. Cheng, H. Sheng, M. Asta, R. O. Ritchie, and E. Ma, *Nat. Commun.* **7**, 13733 (2016).
- ³⁸Z. Lu, W. Jiao, W. H. Wang, and H. Y. Bai, *Phys. Rev. Lett.* **113**, 045501 (2014).
- ³⁹K. A. Dahmen, Y. Ben-Zion, and J. T. Uhl, *Nat. Phys.* **7**, 554 (2011).
- ⁴⁰P. Bak, C. Tang, and K. Wiesenfeld, *Phys. Rev. Lett.* **59**, 381 (1987).
- ⁴¹P. Bak, C. Tang, and K. Wiesenfeld, *Phys. Rev. A* **38**, 364 (1988).
- ⁴²W. Bauer and G. F. Bertsch, *Phys. Rev. Lett.* **65**, 2213 (1990).
- ⁴³D. Amitrano, *Eur. Phys. J. Spec. Top.* **205**, 199 (2012).
- ⁴⁴E. K. H. Salje, A. Saxena, and A. Planes, *Avalanches in Functional Materials and Geophysics* (Springer International Publishing, 2017).
- ⁴⁵K. Chen, P. B. Bak, and S. P. Obukhov, *Phys. Rev. A* **43**, 625 (1991).
- ⁴⁶J. G. Wang, D. Q. Zhao, M. X. Pan, W. H. Wang, S. X. Song, and T. G. Nieh, *Scr. Mater.* **62**, 477 (2010).
- ⁴⁷W. L. Johnson and K. Samwer, *Phys. Rev. Lett.* **95**, 195501 (2005).
- ⁴⁸W. H. Wang, *Prog. Mater. Sci.* **57**, 487 (2012).
- ⁴⁹X. L. Bian, G. Wang, H. C. Chen, L. Yan, J. G. Wang, Q. Wang, P. F. Hu, J. L. Ren, K. C. Chan, N. Zheng, A. Teresiak, Y. L. Gao, Q. J. Zhai, J. Eckert, J. Beadsworth, K. A. Dahmen, and P. K. Liaw, *Acta Mater.* **106**, 66 (2016).
- ⁵⁰J. F. Wang, R. Li, N. B. Hua, and T. Zhang, *J. Mater. Res.* **26**, 2072 (2011).
- ⁵¹A. S. Argon, *Acta Metall.* **27**, 47 (1979).
- ⁵²R. Huang, Z. Suo, J. H. Prevost, and W. D. Nix, *J. Mech. Phys. Solids* **50**, 1011 (2002).
- ⁵³W. H. Wang, *J. Appl. Phys.* **110**, 053521 (2011).
- ⁵⁴A. S. Argon, J. Megusar, and N. J. Grant, *Scr. Metall.* **19**, 591 (1985).
- ⁵⁵K. M. Flores and R. H. Dauskardt, *Acta Mater.* **49**, 2527 (2001).
- ⁵⁶L. Wang, H. Bei, Y. F. Gao, and T. G. Nieh, *Acta Mater.* **59**, 2858 (2011).
- ⁵⁷H. Dai, G. Chen, Q. Fang, and J. Yin, *Appl. Phys. A* **122**, 804 (2016).
- ⁵⁸D. X. Han, G. Wang, J. Li, K. C. Chan, S. To, F. F. Wu, Y. L. Gao, and Q. J. Zhai, *J. Mater. Sci. Technol.* **31**, 153 (2015).
- ⁵⁹M. Q. Jiang and L. H. Dai, *Acta Mater.* **57**, 2730 (2009).
- ⁶⁰L. H. Dai, M. Yan, L. F. Liu, and Y. L. Bai, *Appl. Phys. Lett.* **87**, 141916 (2005).
- ⁶¹N. Tounsi, J. Vincenti, A. Otho, and M. A. Elbestawi, *Int. J. Mach. Tools Manu.* **42**, 1373 (2002).
- ⁶²M. Heggen, F. Spaepen, and M. Feuerbacher, *J. Appl. Phys.* **97**, 033506 (2005).